PHYSICAL REVIEW A **90**, 012302 (2014)

Strong driving of a single spin using arbitrarily polarized fields

P. London,[1,*] P. Balasubramanian,[2] B. Naydenov,[2] L. P. McGuinness,[2,†] and F. Jelezko[2]
[1]*Department of Physics, Technion, Israel Institute of Technology, Haifa 32000, Israel*
[2]*Institut für Quantenoptik, Universitat Ulm, 89073 Ulm, Germany*
(Received 28 April 2014; published 2 July 2014)

The strong-driving regime occurs when a quantum two-level system is driven with an external field whose amplitude is greater than or equal to the energy splitting between the system's states and is typically identified with the breaking of the rotating wave approximation (RWA). We report an experimental study in which the spin of a single nitrogen-vacancy (NV) center in diamond is strongly driven with microwave fields of arbitrary polarization. We measure the NV center spin dynamics beyond the RWA and characterize the limitations of this technique for generating high-fidelity quantum gates. Using circularly polarized microwave fields, the NV spin can be harmonically driven in its rotating frame regardless of the field amplitude, thus allowing rotations around arbitrary axes. Our approach can effectively remove the RWA limit in quantum-sensing schemes and assist in increasing the number of operations in QIP protocols.

DOI: 10.1103/PhysRevA.90.012302 PACS number(s): 03.67.Lx, 67.30.hj, 76.30.Mi

I. INTRODUCTION

The nitrogen-vacancy (NV) center is one of the leading platforms for QIP applications [1,2] and room-temperature quantum metrology [3,4]. Additionally, it serves as a probe for the classical and quantum dynamics of a mesoscopic bath of spins [5,6]. These applications provide great motivation for controlling, and specifically shortening, the manipulation duration of the spin. In QIP, shortening of the gate duration allows an increase in the number of quantum gates applied during the coherence time, T_2, and thus scales up the computational performance [7]. Ultimately, the elementary gate duration defines the processing clock speed [8]; for systems on parity for the number-of-operations figure of merit, it distinguishes between "slow" systems, such as cold trapped atoms and nuclear spins, and "fast" systems, such as semiconductor quantum dots and superconducting flux qubits. In quantum metrology, designed rotations of qubits are used to map the signal (the phase between eigenstates) to a measurable population difference. Specifically, in dynamical decoupling (DD)–based quantum sensing schemes, the qubit may be driven continuously or pulsed at intervals, allowing suppression of noise sources with a slower spectrum than the driving speed or interpulse spacing [9–11]. Thus, the maximum driving speed or pulse duration places an upper bound on the ability to shift the sensing frequencies higher and away from the dominant low-frequency noise [12] and limits the bandwidth of these schemes.

For these goals, and crucially in room-temperature applications, the NV spin is usually manipulated with an oscillatory microwave (MW) field, $B_x(t) = B_1 \cos(\omega t)$ (where B_1 and ω are the field amplitude and frequency, respectively), resonant with the energy splitting of the spin $\hbar\omega_L$, i.e. $\omega = \omega_L$. Then, in a frame rotating with the MW field, the spin is driven by a constant magnetic field, $B_+ = B_1/2$ (corotating field), and an additional rotating field, $B_- = (B_1/2)e^{2i\omega t}$ (counter-rotating field). As long as γB_1 is small compared to ω (where γ is the magnetic moment of the spin), the counter-rotating field can be neglected, an approximation known as the rotating wave approximation (RWA). In this regime, the gate time depends linearly on the inverse of the applied magnetic field amplitude B_1.

However, when the driving amplitude is increased so that γB_1 becomes comparable to the spin's Larmor frequency ω_L, the dynamics manifest complexities due to an interplay of the two fields: the gate fidelity degrades, the rotation (gate) time no longer scales linearly with $1/B_1$, and the dynamics show a pronounced sensitivity to the phase of $B_x(t)$ with respect to the pulse edges [13]. In this regime, known as the strong-driving regime, various solutions to regaining control of the system dynamics have been proposed, including anharmonic pulses [14,15], Landau-Zener-assisted transitions [16], and transitions through an ancillary level in a Λ-type configuration [17].

Here we tackle the strong-driving problem using an approach discussed in an early work by Bloch and Siegert [18]. A spin subjected to two orthogonal, resonant MW fields, $B_x = B_1 \cos(\omega_L t)$ and $B_y = B_1 \cos(\omega_L t + \phi)$, will rotate harmonically if $\phi = \pm\pi/2$. Under this condition, the two orthogonal fields can equivalently be described as circularly polarized MW radiation. When the radiation polarization coincides with the spin transition (i.e., when the angular momentum of the radiation field matches the change in spin number), manipulation with a field solely corotating with the spin occurs, leading to full-contrast rotations. The other case, namely, driving a transition with the counter-rotating field (of opposite handedness or polarization), can be viewed as a driving field with a $2\omega_L$ detuning. Only in the strong-driving regime can rotation of the spin occur, albeit with degraded contrast. Recently, this approach was demonstrated with an ensemble of ^{1}H nuclear spins ($I = 1/2$) in an ultralow-field NMR setup [19]. Here, we investigate this approach using experiments on a single NV center, an electronic spin in a diamond with total spin $S = 1$. For an $S = 1$ system, it is possible to address more than one transition spectrally, enabling polarization selective transitions [20]. We drive the NV center with arbitrarily polarized MW radiation, address one of the two-level systems (TLSs), and study its dynamics in the strong-driving regime, namely, when the Rabi frequency is higher than the Larmor frequency.

---

[*] pazl@tx.technion.ac.il
[†] liam.mcguinness@uni-ulm.de

The paper is organized as follows. In Sec. II we describe the experimental setup and present a theoretical description of the general Hamiltonian of the NV $S = 1$ ground state under two MW fields. Section III discusses the dynamics in a low magnetic field, characterized by selective excitation within a dense spectrum of resonances. In Sec. IV we experimentally demonstrate the strong-driving regime for various polarizations and compare the dynamics under linear versus circular polarization. In Sec. V we discuss the results and elaborate on the effect of an axial MW component on the NV dynamics, i.e., a MW field applied parallel to the NV dipole axis.

II. EXPERIMENTAL SETUP FOR POLARIZED MW RADIATION

The experiments were conducted at room temperature, with single NV centers in a type IIa diamond with a (100) surface. To excite NV centers with arbitrarily polarized MW pulses [20] of short duration, we designed a low-Q MW antenna. The antenna comprises two thin copper wires in a cross-configuration, stretched over the diamond surface [Fig. 1(a)]. The wires are connected to two independent MW sources, switches, and amplifiers and are phase-locked to each other. Alternatively, one can apply the fields through an arbitrary waveform generator to gain full control over the MW parameters. With this setup we were able to manipulate individual NV centers, located at distances of ~10–50 μm from the wire crossing, with Rabi frequencies up to 100 MHz. We have found that the position of the NV center with respect to the wires affects the driving performance (see Sec. V). The ideal scenario is illustrated in Fig. 1(a), where the two fields and the NV axis form an orthogonal system.

The Hamiltonian of the NV-center spin, **S**, in the presence of two orthogonal driving fields, B_x and B_y, of equal magnitude and a constant external magnetic field, B_{ext}, can be written as

$$H = DS_z^2 - \gamma B_{\text{ext}} S_z + \Omega e^{i(\omega t + \phi_g)} \hat{\varepsilon} \cdot \mathbf{S} + \text{H.c.}, \tag{1}$$

where $D = (2\pi)\,2.87$ GHz is the zero-field splitting, $\gamma = (2\pi)$ 2.8 MHz/G is the NV magnetic moment, $\hat{\varepsilon} = (1, e^{i\phi}, 0)$ defines the MW polarization, and H.c. stands for Hermitian conjugate. Here, ω, Ω, and ϕ are the MW frequency, NV Rabi frequency ($\Omega = \gamma B_x = \gamma B_y$), and relative MW phase, respectively. The phase ϕ_g is a *global phase* shared by both fields. In the rotating frame, Eq. (1) is rewritten as (see Appendix A)

$$H' = \begin{bmatrix} \Delta_- & 0 & 0 \\ 0 & 0 & 0 \\ 0 & 0 & \Delta_+ \end{bmatrix} + \frac{\Omega}{\sqrt{2}} \begin{bmatrix} 0 & \varepsilon_- & 0 \\ \varepsilon_-^* & 0 & \varepsilon_+ \\ 0 & \varepsilon_+^* & 0 \end{bmatrix} + \frac{\Omega}{\sqrt{2}} \begin{bmatrix} 0 & \varepsilon_+ e^{-2i\omega t} & 0 \\ \varepsilon_+^* e^{2i\omega t} & 0 & \varepsilon_- e^{2i\omega t} \\ 0 & \varepsilon_-^* e^{-2i\omega t} & 0 \end{bmatrix}, \tag{2}$$

where $\varepsilon_\pm = e^{\mp i\phi_g}(1 - ie^{\mp i\phi})/2$. Here $\omega_L^\pm = D \pm \gamma B_{\text{ext}}$ are the transition frequencies, and $\Delta_\pm = \omega_L^\pm - \omega$ their detuning from the MW frequency [Fig. 1(b)]. The second and third terms in Eq. (2) represent the corotating and counter-rotating terms, respectively. Note that Eqs. (1) and (2) hold for arbitrarily (elliptically) polarized fields, however, we assume that the z component of the MW field is 0. We refine this treatment in Sec. V, in discussing the influence of an MW field with nonzero axial component.

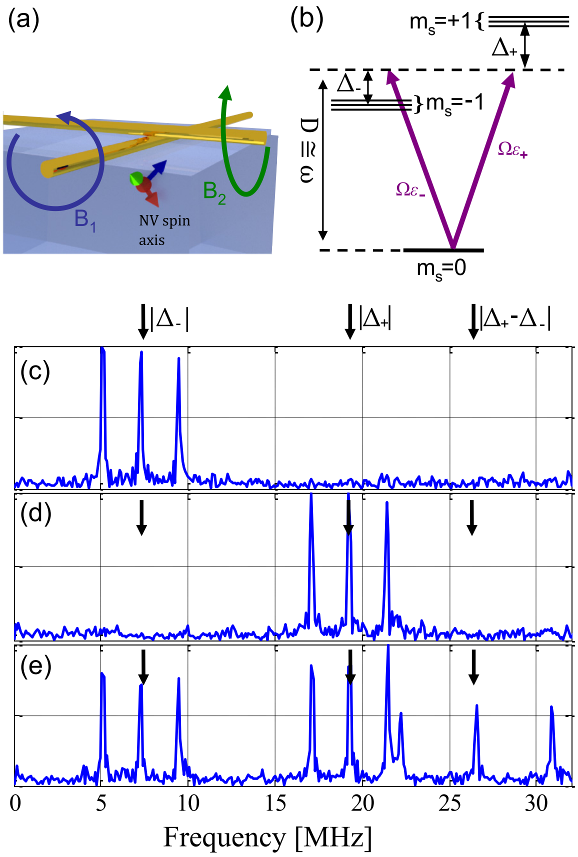

FIG. 1. (Color online) Experimental setup and broadband magnetometry with polarized fields. (a) Microwaves (MWs) transmitted by two crossed wires placed on the diamond surface create orthogonal magnetic fields and, for certain NV positions, allow an arbitrary MW field. (b) Energy scheme of the NV ground state at a low magnetic field. Notations are defined in the text. (c–e) Experimental spectra of Ramsey signals produced with MW $\pi/2$ pulses of right-handed circular polarization (c), left-handed circular polarization (d), and linear polarization (e). Black arrows in (c–e) mark the frequencies $|\Delta_\pm|$ and $|\Delta_+ - \Delta_-|$ at the applied magnetic field.

Next we discuss the dynamics of Eq. (2) in the “low-field” case, where the transitions are nearly degenerate with respect to the Rabi frequency, but the RWA is applicable ($|\Delta_\pm| \ll \Omega \ll \omega$). Then we discuss the dynamics in the “high-field” case, where the transitions are well separated and the Rabi frequency exceeds the transition frequency ($|\Delta_-| \ll \omega \leqslant \Omega$), allowing investigation of a TLS driven beyond the RWA limit.

III. SELECTIVE EXCITATION WITH POLARIZED FIELDS

To characterize the performance of the MW structure we performed broadband Ramsey magnetometry at a low magnetic field, where the $|-1\rangle$ and $|+1\rangle$ states are nearly degenerate [21]. For low-amplitude driving ($\Omega \ll \omega$) one may use the RWA, i.e., assume that the $\varepsilon_\pm e^{\pm 2i\omega t}$ components oscillate many times during the rotation of the spin and, thus, are averaged to 0. Equation (2) then becomes

$$H^{\text{RWA}} = \begin{bmatrix} \Delta_- & (\Omega/\sqrt{2})\varepsilon_- & 0 \\ (\Omega/\sqrt{2})\varepsilon_-^* & 0 & (\Omega/\sqrt{2})\varepsilon_+ \\ 0 & (\Omega/\sqrt{2})\varepsilon_+^* & \Delta_+ \end{bmatrix}. \quad (3)$$

Here we see that $(\Omega/\sqrt{2})\varepsilon_+$ drives the $|0\rangle \longleftrightarrow |+1\rangle$ transition, and $(\Omega/\sqrt{2})\varepsilon_-$ drives the $|0\rangle \longleftrightarrow |-1\rangle$ transition.

First, the NV is optically pumped to the $|0\rangle$ state. Then an MW $\pi/2$ pulse with arbitrary polarization (arbitrary ϕ) manipulates the NV spin to the state $|\psi\rangle = (1/\sqrt{2})[|0\rangle + i\varepsilon_-|-1\rangle + i\varepsilon_+^*|1\rangle]$. This state can be obtained with the evolution operator $U = \exp(iH^{\text{RWA}}t)$, for rotation time t satisfying $(t \cdot \Omega/\sqrt{2}) = \pi/4$, in the limit $\Omega \gg |\Delta_\pm|$. Then, after a free-evolution time τ, the state becomes $|\psi\rangle = (1/\sqrt{2})[|0\rangle + i\varepsilon_- e^{i\Delta_-\tau}|-1\rangle + i\varepsilon_+^* e^{i\Delta_+\tau}|1\rangle]$, and an additional $\pi/2$ pulse with the same polarization gives the final probability of being in the $|0\rangle$ state,

$$P_0(\tau) = \tfrac{1}{2}[1 - |\varepsilon_-|^2\cos(\Delta_-\tau) - |\varepsilon_+|^2\cos(\Delta_+\tau) - |\varepsilon_-|^2|\varepsilon_+|^2(1 - \cos[(\Delta_+ - \Delta_-)\tau])]. \quad (4)$$

The second and third terms oscillate at the MW frequency detuning from the $|0\rangle \longleftrightarrow |-1\rangle$ and $|0\rangle \longleftrightarrow |+1\rangle$ transitions, respectively. The last term oscillates at the frequency separation between the $|\pm 1\rangle$ states and is detuning independent. Using Fourier analysis of $P_0(\tau)$, one can infer the polarization parameters ($|\varepsilon_\pm|^2$) directly, by observing the intensity of each frequency component.

In the experiments, a static axial magnetic field of 4.6 G was used to split the $|\pm1\rangle$ states by 26 MHz, and "hard" $\pi/2$ pulses which efficiently excited both transitions were applied [$\Omega = (2\pi)114$ MHz; note that Ω remained much smaller than $\omega_L \simeq (2\pi)3$ GHz]. By varying the relative phase between the wires, various polarizations could be engineered; left-handed circular polarization [driving the $|0\rangle \rightarrow |-1\rangle$ transition; Fig. 1(c)], right-handed circular polarization [driving the $|0\rangle \rightarrow |+1\rangle$ transition; Fig. 1(d)], and linear polarization [Fig. 1(e)] . In all spectra there is an additional $(2\pi)2.16$-MHz splitting due to a hyperfine interaction with the NV host nitrogen nuclear spin. From the relative amplitudes in the spectral footprint, we deduce that $|\varepsilon_-|^2 = 0.98$, 0.03, and 0.47 (with an error of ±0.05) for Figs. 1(c), 1(d), and 1(e), respectively.

IV. STRONG DRIVING WITH ARBITRARY POLARIZATIONS

After characterizing the MW polarization, we experimentally investigated the strong-driving regime for different applied polarizations. A TLS was prepared using a high axial magnetic field of ~0.1 mT. At this field one finds $\omega_L^- = (2\pi)30$ MHz and $\omega_L^+ = (2\pi)5710$ MHz. For a field resonant with ω_L^-, the far-detuned higher energy transition can be neglected, and the reduced Hamiltonian of the TLS $|0\rangle,|-1\rangle$ [derived from Eq. (2)] is

$$H = \frac{\Omega}{\sqrt{2}}\begin{bmatrix} 0 & \varepsilon_- + \varepsilon_+ e^{-2i\omega_L^- t} \\ \varepsilon_-^* + \varepsilon_+^* e^{2i\omega_L^- t} & 0 \end{bmatrix}, \quad (5)$$

where $(\Omega/\sqrt{2})\varepsilon_-$ is the corotating component of the MW field, and $(\Omega/\sqrt{2})\varepsilon_+ e^{-2i\omega_L^- t}$ is the counter-rotating component. Specifically, for $\phi = \pi/2$, one obtains the Hamiltonian $H = (\Omega/\sqrt{2})\sigma_x$, where σ_x is the Pauli matrix, and the prefactor $\sqrt{2}$ is a remnant of the $S = 1$ nature of the NV system. (The spin interacts more strongly than a true TLS.) This Hamiltonian is exact and independent of the driving-field magnitude, even for $\Omega \geqslant \omega_L^-$, i.e., beyond the RWA limit. The dynamics derived from this Hamiltonian are harmonic oscillations with Rabi frequency Ω. We note that our experiments were conducted with Rabi frequencies of the order of tens of megahertz but, in principle, could be performed in the gigahertz regime with the proper hardware [13]. The approximation leading from Eq. (2) to Eq. (5) breaks only at $\Omega \sim 2D \simeq (2\pi)6$ GHz. For these values parasitic excitations to the $|+1\rangle$ state will interfere with the dynamics.

A. Optimization of the relative phase ϕ

As described above, experimental control of the MW polarization is obtained by tuning the relative phase ϕ between the wires. To further illustrate this control, we performed Rabi oscillations for various relative phases (Fig. 2). We started with a parametric scan in the *weak*-driving regime. The NV spin was driven with both wires, each with amplitude $\Omega = 0.15\omega_L^-$ ([$(2\pi)5.9$ MHz], and the relative phase between the sources was scanned [Fig. 2(a)]. At the optimal phase relation, $\phi = \pi/2$, the NV spin is driven most efficiently, resulting in Rabi oscillations at double the frequency $0.3\omega_L^-$ [Fig. 2(a); dashed (red) line], corresponding to driving with the corotating field, and the counter-rotating term is suppressed completely ($\varepsilon_- = 1$, $\varepsilon_+ = 0$). In contrast, at $\phi = 3\pi/2$ the spin remained untouched [Fig. 2(a); dotted (green) line], as the MW has the opposite polarization to drive the spin transition. Here, the corotating field does not exist ($\varepsilon_- = 0$, $\varepsilon_+ = 1$), and the counter-rotating field can be neglected via the RWA ($\Omega \ll \omega_L^+$). In contrast, in the *strong*-driving regime the spin is also driven by the counter-rotating field [Fig. 2(b)]. Here, we set $\Omega = 0.7\omega_L^-$ for each wire, and only at $\phi = \pi/2$ (representing left-handed circular polarization, σ^-) were pure harmonic oscillations observed, demonstrating Rabi flops with $\Omega = 1.4\omega_L^-$. Hereafter, we denote the ratio of the Rabi frequency to the Larmor frequency$\lambda = \Omega/\omega_L^-$. For other phases, more complex dynamics were observed, accompanied by

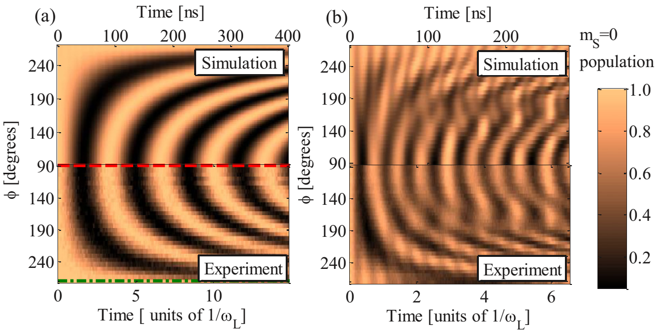

FIG. 2. (Color online) Rabi oscillations with MW fields of various polarizations. Simulated (upper panels) and experimental (lower panels) Rabi oscillations with various phase differences between the wires, in (a) the weak-driving and (b) the strong-driving regimes. In the simulation, an average of 300 initial phases ϕ_g was used.

high-frequency components and lower contrast; specifically, at $\phi > \pi$, the dynamics are governed by the counter-propagating field and one notices an increase in the oscillation frequency with low contrast.

For both cases, a numerical model based on Eq. (5) reproduces the results very well. For all noncircular polarizations, the phase of the MW with respect to the pulse rising edge plays an important role in the dynamics. For example, with linearly polarized MW radiation, the effective driving field is $\tilde{\Omega} = \sqrt{2}\Omega e^{-i(\omega_L^- t-\pi/4)}\cos(\omega_L^- t - \phi_g)$, representing a field with time-dependent magnitude and orientation. Assuming a square pulse shape (the rise and fall times of the experimental pulses were $\sim$1 ns), one finds that for $\phi_g = 0$, the field is $\tilde{\Omega} = \sqrt{2}\Omega\cos(\omega_L^- t)$, and both fields (co- and counter-rotating) start with the maximal amplitude in the same direction (in the rotating frame), effectively rotating the spin instantaneously. In contrast, for $\phi_g = \pi/2$, the effective field is $\tilde{\Omega} = \sqrt{2}\Omega\sin(\omega_L^- t)$. Here, the field has zero amplitude at $t = 0$, and the spin starts to rotate much more slowly, drawing a different trajectory on the Bloch sphere. Conventionally, and in our experiments too, the trigger of the MW switch is not synchronized with the MW source phase, leading to a randomized initial phase ϕ_g over all acquisitions (each sequence was repeated $\sim 10^5$ times for sufficient photon statistics). Therefore, the simulated signal plotted in Fig. 2 is the averaged signal of 300 repetitions of the dynamics under Eq. (5) with uniformly distributed, global phases. In the weak-driving regime the initial MW phase is unimportant and the repeated acquisitions are essentially identical. For more details on the global phase dependence, see Appendix B.

B. Strong driving with linear and circular fields

After optimizing the relative phase for circular polarization ($\phi = \pi/2$) and for linear polarization ($\phi = 0$), we compare the performance of the two polarizations for manipulating the spin in the strong-driving regime. Specifically we compare the ability to steer the spin from the north pole of the Bloch sphere, $|0\rangle$, to the south pole, $|-1\rangle$, i.e., to perform a π pulse.

Figures 3(a), 3(b), and 3(c) show the spin dynamics for $\lambda \sim 0.5$, 1.0, and 1.5, respectively. For extracting the spin projections on the $|0\rangle$ and $|-1\rangle$ states, we have calibrated the photoluminescence level for both states using a relatively weak MW power, ensuring that decoherence mechanisms are not influencing the dynamics. (Typically, the difference in the photoluminescence for these states was $\sim$35%.) A qualitative difference is observed in the spin dynamics as the driving field exceeds the Larmor frequency; the oscillations become anharmonic for linear fields while remaining harmonic for circular fields. We extract two quantities from the measured signals: the time of the first minimum of the signal, t_m, and the $|0\rangle$-state population at this time. The former corresponds to a π-pulse duration for ideal harmonic driving, and the latter corresponds to the π-pulse *fidelity*. We note that our fidelity definition is not the formal one, in which the process fidelity for any arbitrary state is estimated via quantum process tomography [22]. Instead, the probability of being in the $|-1\rangle$ state after the applied gate on the $|0\rangle$ state can sufficiently characterize both the efficiency and the challenges in performing these operations in the strong-driving regime.

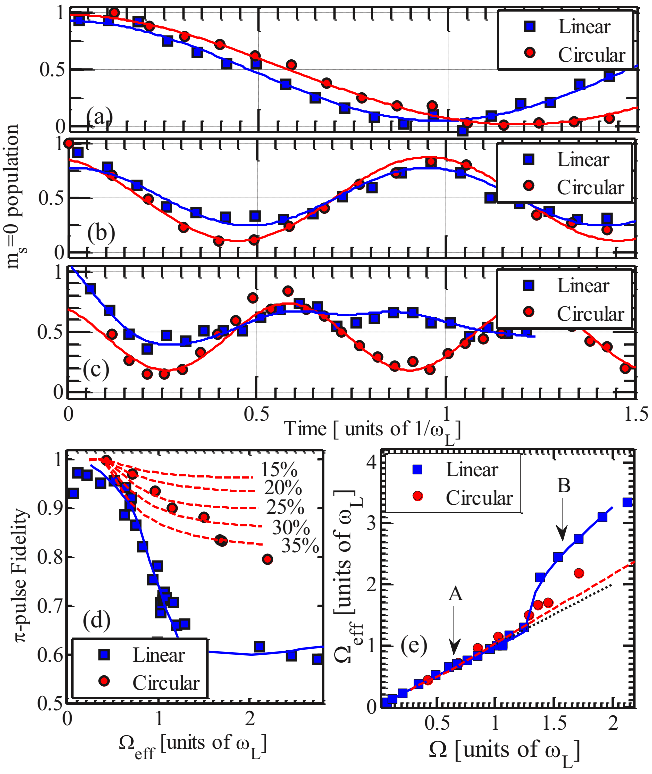

FIG. 3. (Color online) Rabi oscillations with linearly and circularly polarized driving fields. (a–c) Rabi oscillations for various amplitudes of the MW field: experimental data shown as squares for linear fields and as circles for circular fields. Data are presented for (a) $\lambda \simeq 0.5$, (b) $\lambda \simeq 1$, and (c) $\lambda \simeq 1.5$. Solid lines are cosine fits to the circular polarization data and simulated signals from Eq. (5) for the linear polarization data. (d) Experimental comparison of π pulse fidelity for linearly (squares) and circularly (circles) polarized fields. Linear polarization data are modeled with a curve calculated according to Eq. (5) with no fit parameters [solid (blue) curve]. Circular polarzation data are modeled with an additional axial MW field of amplitude 15%–35%Ω [dashed (red) curves]. (e) Effective Rabi frequency vs field amplitude for linearly (squares) and circularly (circles) polarized fields. The ideal dependence for harmonic driving is represented by the dotted line. "A" and "B" labels correspond to Fig. 5(d).

Figure 3(d) shows the fidelity of the π pulse as a function of the effective Rabi strength (defined as half of the inverse of the π-pulse duration, i.e., $\Omega_{\text{eff}} = 1/2t_m$). For linear polarization the π-pulse fidelity decreases substantially when $\lambda \geqslant 1$ [Fig. 3(d); squares], as predicted by a model based on the Schrödinger equation with Eq. (5) [Fig. 3(d); solid line]. In contrast, for circular polarization the fidelity is 93% at $\lambda = 1$. Importantly, the harmonic behavior of the driven spin is still observed for a Rabi frequency twice the Larmor frequency. In principle, the fidelity should not decrease even in the strong-driving regime, however, for high λ values the experimental values show a monotonic reduction in the π-pulse fidelity. This behavior can be partly reproduced by simulations, if an additional field which is applied parallel to the NV axis is included. This is illustrated by the five dashed lines in Fig. 3(d), for which we added to Eq. (5) an

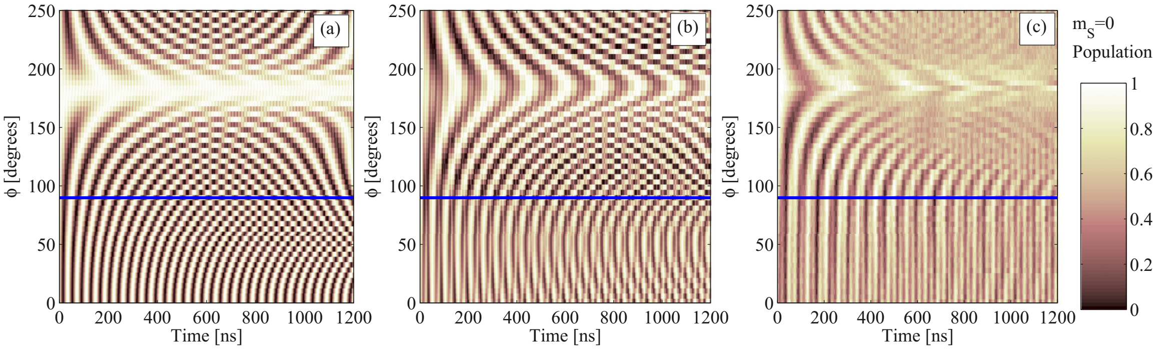

FIG. 4. (Color online) Strong driving of an NV center with a large axial MW field. Simulation of Rabi oscillations [$\omega_L^- = (2\pi)37.8$ MHz, $\Omega_x = \Omega_y = 1.408\omega_L^-$] with (a) $\Omega_z = 0$ and (b) $\Omega_z = 1.67\Omega_x$. (c) Experimental Rabi oscillations for a single NV center with ω_L^- and $\Omega_{x,y}$ equal to the values in the simulations and with a strong axial component.

additional term, $H_\parallel = S_z{\cdot}\Omega_z \cos(\omega_L^- t)$, where S_z is the spin operator in the z axis, and Ω_z is the MW projection on the z axis. The improved agreement between experiment and simulation for values of $\Omega_z/\Omega = 20\%$–30% implies that this could be a dominant mechanism for the degraded performance of circularly polarized radiation as the field amplitude is increased.

An additional figure of merit for the manipulation performance is how the driving speed changes with the applied MW amplitude [Fig. 3(e)]. Here, for a linearly polarized MW field at $\lambda > 1.2$ multiple minima appear in the fluorescence signal (see Appendix B). As a consequence, the time of the first minimum changes abruptly at these values, shifting from the predicted behavior of $\Omega = \Omega_{\text{eff}} = 1/2t_m$ to higher values [Fig. 3(e); squares], in agreement with our numerical model [Fig. 3(e), solid line; the ideal behavior is depicted as the dotted black line]. In contrast, for circular polarization the π-pulse duration follows the ideal behavior [Fig. 3(e); circles], with a small deviation towards higher values. Again, this is partly explained by including an axial field [dashed (red) line], calculated with $\Omega_z/\Omega = 20\%$).

V. DISCUSSION

The comparison of the experiments and simulations in Fig. 3 indicates that an axial MW field could play an important role in our driving scheme. This might not be the only mechanism for the performance degradation: Although the wires were isolated (i.e., no direct Ohmic short was present), we have witnessed a small inductive cross talk between the wires. (When the power was applied through one of the wires, a 90° phase-shifted signal appeared in the other wire.) We estimate this leakage to be bounded by a few percent according to the direct measurement of the output signals, but it results in some ellipticity of the MW field.

Whereas the residual cross talk between the wires cannot be mitigated very easily in our setup, the axial projection of the MW field can be varied simply by measuring NV centers at various positions relative to the cross-wires. We selected an NV center with a high axial component of the MW field, for which a scan of Rabi flops as a function of the relative phase between the wires is shown in Fig. 4. Here, without an axial component of the MW field, one would expect to obtain the results in Fig. 4(a), where at 0° (representing σ^- polarization) the spin is driven by harmonic oscillations by the corotating field. In contrast, the experiment shows a qualitatively different behavior, where for phases in the range 0–90°, the oscillation frequency remains relatively constant, and the shape is clearly anharmonic [the solid (blue) line in Fig. 4 is a guide for the eye]. Moreover, at the cancellation point (180°), the spin is still rotated at a Rabi frequency about one-fifth of the applied Ω [Fig. 4(c)]. Remarkably, a numerical simulation based on Eq. (5) with axial component $S_z\Omega_z$ reproduces these features, elucidating the importance of axial driving for this NV center [Fig. 4(b)]. At the cancellation point, for instance, the spin is likely to be driven via multiple Landau-Zener transitions [16], rather than by conventional Rabi flops.

Thus, the performance of our current design of a polarized MW antenna (cross-wire configuration) in the strong-driving regime is sensitive to the projection of the MW field on the NV-center axis. Although axial driving is important for realizing Landau-Zener-like transitions [16,23,24], it is also accompanied by a reduction in the oscillation contrast.

VI. CONCLUSION AND OUTLOOK

In conclusion, we have studied the dynamics of a single spin under resonant, polarized MW radiation. The relative phase of two MW sources was utilized as a knob to adjust the MW polarization. We have demonstrated high-fidelity selective excitation within a dense spectrum of resonances, allowing individual excitation of adjacent transitions ($\Delta \sim 26$ MHz) with fast pulses of $\Omega \simeq 114$ MHz. This is of importance near level crossings, where conventionally one would have to decrease the driving power to avoid leakage of population to neighboring states or use optimal control solutions [2,25]. Here, the selection rules obtained with circularly polarized light allow selective excitation of degenerate transitions and can be used to determine both the sign and the magnitude of the external magnetic field [26]. We showed that under circular MW fields, the spin experiences pure harmonic oscillations regardless of the applied field strength, specifically even above the RWA limit (in our case more than twice the Larmor frequency). Importantly, although in the strong-driving regime, the spin is still rotated in its rotating frame, allowing for universal control around the Bloch sphere by controlling the global phase of the MW fields ϕ_g. This enables the use of complex dynamical decoupling schemes [27], with a sub-Larmor-period intrapulse duration. Moreover, in continuous wave sensing schemes such as dressed-state magnetometry [28] and Hartmann-Hahn double resonance [29], the spin must be maintained in its dressed state. Here, our scheme overcomes the upper limit to detection frequencies set by the Larmor frequency.

Our current design suffers from the influence of an axial component of the MW field. More versatile stuctures, for example, using two wires to generate each magnetic field $B_{x,y}$ component, could mitigate this problem by allowing cancellation of the axial field without supressing the transverse component. Spin manipulation with an axial field is strongly connected to Landau-Zener transitions [16] and coherent destruction of tunneling [24] and, therefore, is interesting in and of itself. Moreover, our ability to control the magnetic field in all three directions can assist in constructing the Berry Hamiltonian [30] for acquiring controlled geometric phases with a single spin in a diamond without rotating the sample [31].

ACKNOWLEDGMENTS

The authors thank Jochen Scheuer, Xi Kong, and Christoph Müller for assistance with experiments. The authors are grateful to Philip Hemmer, David Gershoni, Ran Fischer, and Chen Avinadav for fruitful discussions and suggestions. The research was supported by DARPA, EU (ERC Synergy grant BioQ, DIAMANT), DFG (Grants No. SFB TR 21, No. FOR 1493, and No. FOR 1482), RSF, and the Alexander von Humboldt and Volkswagen foundations.

APPENDIX A: DERIVATION OF EQ. (2)

We derive the MW terms in the Hamiltonian Eq.(2). The interaction term of the NV spin **S**, with MW field of frequency ω, Rabi frequency Ω, and relative phase ϕ, is

$$H_{\mathrm{MW}} = \Omega(\cos(\omega t)S_x + \cos(\omega t + \phi)S_y),$$

where the transverse spin operators are

$$S_x = \frac{1}{\sqrt{2}}\begin{bmatrix} 0 & 1 & 0 \\ 1 & 0 & 1 \\ 0 & 1 & 0 \end{bmatrix}, \quad S_y = \frac{1}{\sqrt{2}}\begin{bmatrix} 0 & -i & 0 \\ i & 0 & -i \\ 0 & i & 0 \end{bmatrix}.$$

We move into the MW rotating frame using the transformation $H' = i\frac{dU}{dt}U^\dagger - U^\dagger H U$ with $U = \exp(iAt)$ and A is given by

$$A = \begin{bmatrix} \omega & 0 & 0 \\ 0 & 0 & 0 \\ 0 & 0 & \omega \end{bmatrix}.$$

Then the transformation operators are

$$U = \begin{bmatrix} e^{i\omega t} & 0 & 0 \\ 0 & 1 & 0 \\ 0 & 0 & e^{i\omega t} \end{bmatrix}, \quad U^\dagger = \begin{bmatrix} e^{-i\omega t} & 0 & 0 \\ 0 & 1 & 0 \\ 0 & 0 & e^{-i\omega t} \end{bmatrix},$$

and the spin operators transform according to

$$U^\dagger S_x U = \frac{1}{\sqrt{2}}\begin{bmatrix} e^{-i\omega t} & 0 & 0 \\ 0 & 1 & 0 \\ 0 & 0 & e^{-i\omega t} \end{bmatrix}\begin{bmatrix} 0 & 1 & 0 \\ 1 & 0 & 1 \\ 0 & 1 & 0 \end{bmatrix}\begin{bmatrix} e^{i\omega t} & 0 & 0 \\ 0 & 1 & 0 \\ 0 & 0 & e^{i\omega t} \end{bmatrix} = \frac{1}{\sqrt{2}}\begin{bmatrix} 0 & e^{-i\omega t} & 0 \\ e^{i\omega t} & 0 & e^{i\omega t} \\ 0 & e^{-i\omega t} & 0 \end{bmatrix},$$

$$U^\dagger S_y U = \frac{1}{\sqrt{2}}\begin{bmatrix} e^{-i\omega t} & 0 & 0 \\ 0 & 1 & 0 \\ 0 & 0 & e^{-i\omega t} \end{bmatrix}\begin{bmatrix} 0 & -i & 0 \\ i & 0 & -i \\ 0 & i & 0 \end{bmatrix}\begin{bmatrix} e^{i\omega t} & 0 & 0 \\ 0 & 1 & 0 \\ 0 & 0 & e^{i\omega t} \end{bmatrix} = \frac{1}{\sqrt{2}}\begin{bmatrix} 0 & -ie^{-i\omega t} & 0 \\ ie^{i\omega t} & 0 & -ie^{i\omega t} \\ 0 & ie^{-i\omega t} & 0 \end{bmatrix}.$$

The terms in the Hamiltonian are calculated as

$$\Omega\cos(\omega t)\,U^\dagger S_x U = \Omega\frac{1}{2}(e^{i\omega t} + e^{-i\omega t})\frac{1}{\sqrt{2}}\begin{bmatrix} 0 & e^{-i\omega t} & 0 \\ e^{i\omega t} & 0 & e^{i\omega t} \\ 0 & e^{-i\omega t} & 0 \end{bmatrix} = \frac{\Omega}{2\sqrt{2}}\begin{bmatrix} 0 & 1 + e^{-2i\omega t} & 0 \\ 1 + e^{2i\omega t} & 0 & 1 + e^{2i\omega t} \\ 0 & 1 + e^{-2i\omega t} & 0 \end{bmatrix},$$

$$\begin{aligned}\cos(\omega t + \phi)U^\dagger S_y U &= \Omega\frac{1}{2}(e^{i(\omega t+\phi)} + e^{-i(\omega t+\phi)})\frac{1}{\sqrt{2}}\begin{bmatrix} 0 & -ie^{-i\omega t} & 0 \\ ie^{i\omega t} & 0 & -ie^{i\omega t} \\ 0 & ie^{-i\omega t} & 0 \end{bmatrix} \\ &= \frac{\Omega}{2\sqrt{2}}\begin{bmatrix} 0 & -i(e^{i\phi} + e^{-i(2\omega t+\phi)}) & 0 \\ i(e^{i(2\omega t+\phi)} + e^{-i\phi}) & 0 & -i(e^{i(2\omega t+\phi)} + e^{-i\phi}) \\ 0 & i(e^{i\phi} + e^{-i(2\omega t+\phi)}) & 0 \end{bmatrix},\end{aligned}$$

and combining the two terms, we write the Hamiltonian in the MW rotating frame $H'_{\mathrm{MW}} = U^{\dagger}[\Omega \cos(\omega t) S_x + \cos(\omega t + \phi) S_y] U$:

$$
\begin{aligned}
H'_{\mathrm{MW}} &= \frac{\Omega}{2\sqrt{2}} \begin{bmatrix} 0 & 1 + e^{-2i\omega t} & 0 \\ 1 + e^{2i\omega t} & 0 & 1 + e^{2i\omega t} \\ 0 & 1 + e^{-2i\omega t} & 0 \end{bmatrix} \\
&\quad + \frac{\Omega}{2\sqrt{2}} \begin{bmatrix} 0 & -i(e^{i\phi} + e^{-i(2\omega t + \phi)}) & 0 \\ i(e^{i(2\omega t+\phi)} + e^{-i\phi}) & 0 & -i(e^{i(2\omega t+\phi)} + e^{-i\phi}) \\ 0 & i(e^{i\phi} + e^{-i(2\omega t+\phi)}) & 0 \end{bmatrix} \\
&= \frac{\Omega}{\sqrt{2}} \begin{bmatrix} 0 & \varepsilon_- & 0 \\ \varepsilon_-^* & 0 & \varepsilon_+ \\ 0 & \varepsilon_+^* & 0 \end{bmatrix} + \frac{\Omega}{\sqrt{2}} \begin{bmatrix} 0 & e^{-2i\omega t}\varepsilon_+ & 0 \\ e^{2i\omega t}\varepsilon_+^* & 0 & e^{2i\omega t}\varepsilon_- \\ 0 & e^{-2i\omega t}\varepsilon_-^* & 0 \end{bmatrix},
\end{aligned}
$$

where in the last row we assigned $\varepsilon_{\pm} = e^{\mp i\phi_g}(1 - ie^{\mp i\phi})/2$.

APPENDIX B: GLOBAL PHASE DEPENDENCE IN LINEAR POLARIZATION DATA

Figures 3(d) and 3(e) present the analysis of Rabi oscillations with a linear polarized MW field: the population transfer at the first minimum point in the signal decreases substantially as the Rabi frequency increases, and the π-pulse duration (the evolution time until the first minimum) changes when the RWA is exceeded. In contrast, in Ref. [13] it is found that close-to-unity population transfer can occur also in the strong-driving regime and that the π-pulse duration is very hard to predict. The contradiction arises from the experimental technique which was used in our work, namely, averaging many realizations of the MW phase at the pulse rising edge, ϕ_g. In [13]–[15], the MW phase was synchronized to the pulse edge. While our technique suppresses the sensitivity to imperfections in the driving system, it introduces a systematic reduction in the driving performances. It is worth mentioning that there is no systematic deterioration when applying strong *circular* MW fields. Here we describe the global-phase dependence using numerical simulations, compared with the measured Rabi oscillation signals. Figures 5(a)–5(c) show the associated dynamics for various field strengths and for various ϕ_g values. At $\lambda = 0.1$ [Fig. 5(a)], the influence of the counter-rotating term is negligible and the dynamics is identical for any ϕ_g at the appropriated rotating frame [dashed (red) curves]. Then the spin rotates around a big circle on the Bloch sphere. At $\lambda = 0.33$ [Fig. 5(b)], the dynamics changes for each ϕ_g, but the averaged time trace still resembles harmonic oscillations [solid (blue) curve]. This demonstrates the robustness of the averaging technique. At the higher Rabi frequency $\lambda = 1.2$ [Fig. 5(c)], the counter-rotating term influences the spin rotations markedly, and for each ϕ_g the dynamics is complete different; while for a given ϕ_g, complete population transfer from $\langle\sigma_Z\rangle = +1$ to $\langle\sigma_Z\rangle = -1$ can occur [Fig. 5(c); thick dashed (red) curve] for the ensemble average of many ϕ_g, the population transfer does not exceed 60%, demonstrating the downside of this technique. When averaging many ϕ_g realizations, the principal minimum point of the signal, which marks the π-pulse operation, changes into a multiple-minimum structure, as shown in Fig. 5(d). Circles and rectangles are experimental values measured at $\lambda = 1.2$ and 1.4, respectively. Solid lines are the results of a numerical simulation averaging 300 different ϕ_g values. From the Bloch sphere representation it is clear that at these values the averaged spin state becomes mixed (red and blue curves) compared to the rotation in the weak-driving regime (green curve). In Fig. 5(d), we have labeled points A and B, which are addressed in the text and in Fig. 3.

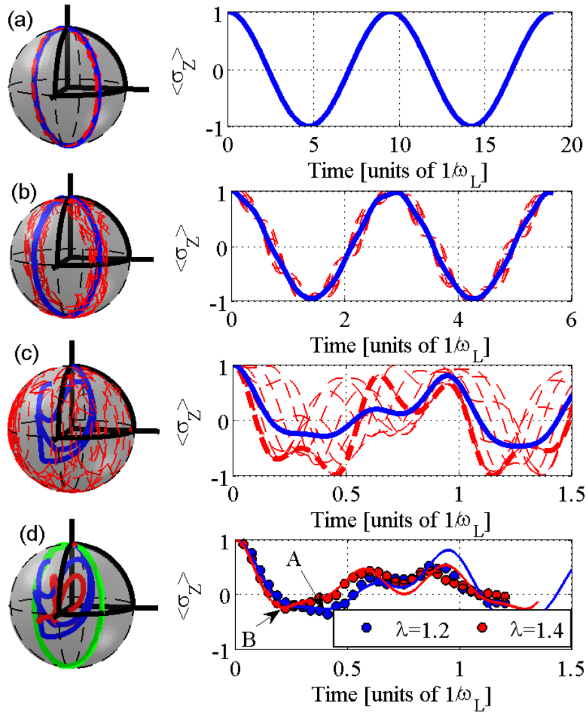

FIG. 5. (Color online) Global phase dependence in the strong-driving regime. (a–c) Rabi oscillations for increasing Rabi-frequency values, $\lambda = 0.1$ (a), $\lambda = 0.33$ (b), and $\lambda = 1.2$ (c). Left: Bloch sphere representation of the spin state. Right: The spin's z component as a function of the driving duration. Dashed (red) curves are various realizations of ϕ_g, and the solid (blue) curve is an averaged trajectory over 300 realizations. (d) Comparison between experimental values (circles and squares) and numerical simulations for high λ values (1.2, and 1.4, respectively); the green curve represents Rabi oscillations in the weak-driving regime and serves as a guide for the eye.

[1] T. D. Ladd, F. Jelezko, R. Laflamme, Y. Nakamura, C. Monroe, and J. L. O'Brien, Nature **464**, 45 (2010).
[2] G. Waldherr, Y. Wang, S. Zaiser, M. Jamali, T. Schulte-Herbruggen, H. Abe, T. Ohshima, J. Isoya, J. F. Du, P. Neumann, and J. Wrachtrup, Nature **506**, 204 (2014).
[3] H. J. Mamin, M. Kim, M. H. Sherwood, C. T. Rettner, K. Ohno, D. D. Awschalom, and D. Rugar, Science **339**, 557 (2013).
[4] T. Staudacher, F. Shi, S. Pezzagna, J. Meijer, J. Du, C. A. Meriles, F. Reinhard, and J. Wrachtrup, Science **339**, 561 (2013).
[5] G. de Lange, T. van der Sar, M. Blok, Z.-H. Wang, V. Dobrovitski, and R. Hanson, Sci. Rep. **2**, 382 (2012).
[6] F. Reinhard, F. Shi, N. Zhao, F. Rempp, B. Naydenov, J. Meijer, L.T. Hall, L. Hollenberg, J. Du, R.B. Liu, and J. Wrachtrup, Phys. Rev. Lett. **108**, 200402 (2012).
[7] T. H. Taminiau, J. Cramer, T. van der Sar, V. V. Dobrovitski, and R. Hanson, Nature Nanotech. **9**, 171 (2014).
[8] D. Press, T. D. Ladd, B. Zhang, and Y. Yamamoto, Nature **456**, 218 (2008).
[9] T. H. Taminiau, J. J. T. Wagenaar, T. van der Sar, F. Jelezko, V. V. Dobrovitski, and R. Hanson, Phys. Rev. Lett. **109**, 137602 (2012).
[10] S. Kolkowitz, Q. P. Unterreithmeier, S. D. Bennett, and M. D. Lukin, Phys. Rev. Lett. **109**, 137601 (2012).
[11] J. R. Maze, P. L. Stanwix, J. S. Hodges, S. Hong, J. M. Taylor, and P. Cappellaro, L. Jiang, M. V. G. Dutt, E. Togan, A. S. Zibrov, A. Yacoby, R. L. Walsworth, and M. D. Lukin, Nature **455**, 644 (2008).
[12] Y. Romach, C. Mueller, T. Unden, L. J. Rogers, T. Isoda, K. M. Itoh, M. Markham, A. Stacey, J. Meijer, S. Pezzagna, B. Naydenov, L. P. McGuinness, N. Bar-Gill, and F. Jelezko, arXiv:1404.3879.
[13] G. D. Fuchs, V. V. Dobrovitski, D. M. Toyli, F. J. Heremans, and D. D. Awschalom, Science **326**, 1520 (2009).
[14] C. Avinadav, R. Fischer, P. London, and D. Gershoni, Phys. Rev. B **89**, 245311 (2014).
[15] J. Scheuer, X. Kong, R. S. Said, J. Chen, A. Kurz, L. Marseglia, J. Du, P. R. Hemmer, S. Montangero, T. Calarco, B. Naydenov, and F. Jelezko, arXiv:1309.4399.
[16] J. Zhou, P. Huang, Q. Zhang, Z. Wang, T. Tan, X. Xu, F. Shi, X. Rong, S. Ashhab, and J. Du, Phys. Rev. Lett. **112**, 010503 (2014).
[17] Y. Kodriano, I. Schwartz, E. Poem, Y. Benny, R. Presman, T. A. Truong, P. M. Petroff, and D. Gershoni, Phys. Rev. B **85**, 241304(R) (2012).
[18] F. Bloch and A. Siegert, Phys. Rev. **57**, 522 (1940).
[19] J. H. Shim, S. J. Lee, K. K. Yu, S. M. Hwang, and K. Kim, J. Magn. Reson. **239**, 87 (2014).
[20] T. P. M. Alegre, C. Santori, G. Medeiros-Ribeiro, and R. G. Beausoleil, Phys. Rev. B **76**, 165205 (2007).
[21] C. Zhuo-liang, Chin. Phys. Lett. **14**, 352 (1997).
[22] M. A. Nielsen and I. L. Chuang, *Quantum Computation and Quantum Information (Cambridge Series on Information and the Natural Sciences)* (Cambridge University Press, Cambridge, 2000).
[23] G. D. Fuchs, G. Burkard, P. V. Klimov, and D. D. Awschalom, Nat. Phys. **7**, 789 (2011).
[24] L. Childress and J. McIntyre, Phys. Rev. A **82**, 033839 (2010).
[25] F. Dolde, V. Bergholm, Y. Wang, I. Jakobi, B. Naydenov, S. Pezzagna, J. Meijer, F. Jelezko, P. Neumann, T. Schulte-Herbrüggen, J. Biamonte, and J. Wrachtrup, Nat. Commun. **5**, 3371 (2014).
[26] J. Michl, T. Teraji, S. Zaiser, I. Jakobi, G. Waldherr, F. Dolde, P. Neumann, M. W. Doherty, N. B. Manson, J. Isoya, and J. Wrachtrup, Appl. Phys. Lett. **104**, 102407 (2014).
[27] T. Gullion, D. B. Baker, and M. S. Conradi, J. Magn. Reson., Ser. (1969) **89**, 479 (1990).
[28] M. Loretz, T. Rosskopf, and C. L. Degen, Phys. Rev. Lett. **110**, 017602 (2013).
[29] P. London, J. Scheuer, J. M. Cai, I. Schwarz, A. Retzker, M. B. Plenio, M. Katagiri, T. Teraji, S. Koizumi, J. Isoya, R. Fischer, L. P. McGuinness, B. Naydenov, and F. Jelezko, Phys. Rev. Lett. **111**, 067601 (2013).
[30] M. V. Berry, Proc. R. Soc. Lond. A **392**, 45 (1984).
[31] D. Maclaurin, M. W. Doherty, L. C. L. Hollenberg, and A. M. Martin, Phys. Rev. Lett. **108**, 240403 (2012).